An Edge-Based Formulation for Combined-Cycle Units

Lei Fan, *Student Member, IEEE*, and Yongpei Guan, *Senior Member, IEEE*

***Abstract*—As the number of combined-cycle units increases, efficient modeling approaches for these units play important roles for independent system operators (ISOs). Based on various combinations of combustion turbines (CTs) and steam turbines (STs), the combined-cycle unit could work at different configurations (modes) with different efficiencies. In this paper, we propose an edge-based formulation for the combined-cycle units in the unit commitment problem to improve the accuracy and effectiveness of current modeling approaches. Our formulation can 1) clearly describe the transition processes among different configurations so as to satisfy the ISO financial offer submission requirements and (2) capture physical constraints of each turbine, including the exact min-up/down time and time dependent startup cost, in the combined-cycle units so as to increase the operational flexibility while ensuring system feasibility. This model fits well with the current U.S. deregulated electricity market. The final numerical studies show that our approaches perform better than the current configuration-based modeling approach.**

***Index Terms*—Combined-cycle units, mixed-integer linear programming formulation, unit commitment.**

NOMENCLATURE

A. Sets

$\mathcal{B}$	Set of buses.
$\mathcal{E}_k$	Set of all edges in the state transition graph of combined-cycle unit k.
$\mathcal{E}^{\mathrm{all}}_{m,k}$	Set of all edges connected to mode m for combined-cycle unit k.
$\mathcal{E}^{\mathrm{in}}_{m,k}$	Set of incoming edges of mode m for combined-cycle unit k.
$\mathcal{E}^{\mathrm{out}}_{m,k}$	Set of outgoing edges of mode m for combined-cycle unit k.
$\mathcal{E}^{\mathrm{sl}}_{m,k}$	Set of self-loop edges of mode m for combined-cycle unit k.
$\mathcal{E}^{\mathrm{sd}}_{i,k}$	Set of edges where turbine i in combined-cycle unit k shuts down.
$\mathcal{E}^{\mathrm{su}}_{i,k}$	Set of edges where turbine i in combined-cycle unit k starts up.
$\mathcal{G}^{\mathrm{C}}$	Set of combined-cycle units.
$\mathcal{G}^{\mathrm{C}}_b$	Set of combined-cycle units at bus b.
$\mathcal{G}^{\mathrm{CT}}_k$	Set of CTs in combined-cycle unit k.
$\mathcal{G}^{\mathrm{ST}}_k$	Set of STs in combined-cycle unit k.
$\mathcal{G}^{\mathrm{T}}$	Set of traditional thermal units.
$\mathcal{G}^{\mathrm{T}}_b$	Set of traditional thermal units at bus b.
$\mathcal{L}$	Set of transmission lines.
$\mathcal{M}_k$	Set of modes in the state transition graph for combined-cycle unit k.
$\mathcal{M}^{\mathrm{off}}_{i,k}$	Set of modes where turbine i in combined-cycle unit k is offline.
$\mathcal{M}^{\mathrm{on}}_{i,k}$	Set of modes where turbine i in combined-cycle unit k is online.
$\mathcal{T}$	Set of operation time span.

B. Parameters

$C_{b,l}$	Transmission capacity of transmission line from bus b to bus l (MW).
C^{QSC}_k	Quick start capacity of combined-cycle unit k (MW).
C^{QST}_n	Quick start capacity of traditional thermal unit n (MW).
D^t_b	Load at bus b at time period t (MW).
D^t	System load at time period t (MW).
$P^{\min}_{m,k}$	Minimum generation amount of mode m of combined-cycle unit k (MW).
$P^{\min}_n$	Minimum generation amount of traditional thermal unit n (MW).
$P^{\max}_{m,k}$	Maximum generation amount of mode m of combined-cycle unit k (MW).
$P^{\max}_n$	Maximum generation amount of traditional thermal unit n (MW).
P^{cap}_k	Total capacity of combined-cycle unit k (MW).
$R^{\mathrm{D}}_{e,k}$	Ramp-down limit at edge e of combined-cycle unit k (MW/h).
$\overline{R}^{\mathrm{D}}_n$	Ramp-down limit of traditional thermal unit n at shut-down stage (MW/h).
R^{D}_n	Ramp-down limit of traditional thermal unit n (MW/h).
$R^{\mathrm{MC}}_{m,k}$	Sustained ramp limit of mode m of combined-cycle unit k (MW/min).
R^{MT}_n	Sustained ramp limit of traditional thermal unit n (MW/min).
$R^{\mathrm{U}}_{e,k}$	Ramp-up limit at edge e of combined-cycle unit k (MW/h).
$\overline{R}^{\mathrm{U}}_n$	Ramp-up limit of traditional thermal unit n at start-up stage (MW/h).
R^{U}_n	Ramp-up limit of traditional thermal unit n (MW/h).

Manuscript received August 31, 2014; revised December 05, 2014, March 16, 2015, and May 29, 2015; accepted May 30, 2015. Date of publication August 05, 2015; date of current version April 15, 2016. Paper no. TPWRS-01189-2014.

The authors are with the Department of Industrial and Systems Engineering, University of Florida, Gainesville, FL 32611 USA (e-mail: guan@ise.ufl.edu).

Color versions of one or more of the figures in this paper are available online at http://ieeexplore.ieee.org.

Digital Object Identifier 10.1109/TPWRS.2015.2443036

RO^t System operating reserve amount at time period t (MW).
RS^t System spinning reserve amount at time period t (MW).
SU_n Start-up cost of traditional thermal unit n ($).
$\mathrm{SU}_{i,k}$ Start-up cost of turbine i in combined-cycle unit k ($).
SD_n Shut-down cost of traditional thermal unit n ($).
$\mathrm{SD}_{i,k}$ Shut-down cost of turbine i in combined-cycle unit k ($).
$T_{i,k}^{\mathrm{cold}}$ Cold start time of turbine i in combined-cycle unit k (h).
$T_{i,k}^{\mathrm{warm}}$ Warm start time of turbine i in combined-cycle unit k (h).
$T_{i,k}^{\mathrm{C,minu}}$ Min-up time for turbine i in combined-cycle unit k (h).
$T_{i,k}^{\mathrm{C,mind}}$ Min-down time for turbine i in combined-cycle unit k (h).
$T_n^{\mathrm{T,minu}}$ Min-up time for traditional thermal unit n (h).
$T_n^{\mathrm{T,mind}}$ Min-down time for traditional thermal unit n (h).
$X_{b,l}$ Reactance of transmission line from bus b to bus l (p.u.).

C. Binary Decision Variables

u_n^t Start-up status of traditional thermal unit n at time period t.
v_n^t Shut-down status of traditional thermal unit n at time period t.
$w_{e,k}^t$ Status of edge e of the transition graph for combined-cycle unit k at time period t.
y_n^t On/Off status of traditional thermal unit n at time period t.

D. Continuous Decision Variables

fc_k^t Generation cost of combined-cycle unit k at time period t ($).
ft_n^t Generation cost of traditional thermal unit n at time period t ($).
$fc_{m,k}^t$ Generation cost of mode m of combined-cycle unit k at time period t ($).
orc_k^t Operating reserve of combined-cycle unit k at time period t (MW).
ort_n^t Operating reserve of traditional thermal unit n at time period t (MW).
src_k^t Spinning reserve of combined-cycle unit k at time period t (MW).
srt_n^t Spinning reserve of traditional thermal unit n at time period t (MW).
$suc_{i,k}^t$ Start-up cost of turbine i in combined-cycle unit k at time period t ($).
$sdc_{i,k}^t$ Shut-down cost of turbine i in combined-cycle unit k at time period t ($).
tc_k^t Transition cost of combined-cycle unit k at time period t ($).
$p_{m,k}^t$ Output of mode m of combined-cycle unit k at time period t (MW).
p_k^t Output of combined-cycle unit k at time period t (MW).
p_n^t Output of traditional thermal unit n at time period t (MW).
θ_b^t The phase angle at bus b at time period t (rad).

I. Introduction

THE utilization of gas-fired power plants has been increasing in recent years due to 1) the lower natural gas price [1], 2) fewer emissions and higher electrical efficiency (50%–59%) at nominal output of gas-fired generators (see, e.g., [2] and [3], respectively), and 3) fast response ability and operational flexibility (more details on the utilization of the multi-mode operation of a combined-cycle unit can be found in [4]). It is projected that combined-cycle units will share around 26% of total U.S. power generation by 2018 [5].

However, the complexity of the operation of a combined-cycle unit brings challenges to the modeling of the problem. Four typical ways to model the operations of combined-cycle units have been investigated in the literature (see [6], [7], and [8]). The first approach is the aggregated modeling approach, which treats the whole combined-cycle unit as a traditional thermal unit. The second approach, named the pseudo unit approach, associates each combustion turbine (CT) with a portion of the steam turbine (ST). The third approach is called the configuration-based approach, which represents each combination of CTs and STs as a configuration. The fourth approach is named the component-based approach, which describes physical constraints for each individual CT and ST. The dependency relationship among CTs and STs is represented by a group of constraints.

For current deregulated electricity market practice, independent system operators (ISOs) take the main role in developing and evaluating the combined-cycle unit models. Most ISOs (e.g., MISO [5], NYISO [6], PJM [7], and ISO-NE [9]) take an aggregate modeling or pseudo unit approach. However, the aggregated modeling approach cannot capture most physical constraints for each CT or ST, which can make it physically impossible to implement the unit commitment decisions decided by this approach in practice [10]. For example, the aggregated modeling approach does not describe the transition process among different configurations (combinations of CTs and STs), because this approach treats the whole combined-cycle unit as a traditional thermal unit. In addition, the pseudo unit approach results in an unrealistic operational range because of its simple representation. Meanwhile, ISOs start to use the configuration-based modeling approach considering day-ahead offer submission convenience. For instance, the day-ahead offers should be submitted in terms of configurations, and each ISO will decide which configuration is committed. This configuration-based modeling approach has been implemented in the day-ahead market in CAISO and ERCOT (see [10], [11], and [12]). MISO is also developing the configuration-based model [5]. Finally, the component-based approach is more suitable for network security applications [13].

Although the configuration-based model has been increasingly used in practice for the day-ahead market, there are

limitations on this approach. When one or more turbines start up or shut down, the combined-cycle unit transitions from one configuration to another. The cost of this transition is essentially the sum of the start-up or shut-down costs of the related turbines. Current configuration-based modeling approaches cannot exactly provide this cost, because they cannot capture the status of each turbine at the time of the transition [14]. In addition, it is difficult for this approach to describe the min-up/down time restrictions of each individual CT and ST in a combined-cycle unit. In this paper, we propose an edge-based modeling approach to strengthen this configuration-based modeling approach. Our proposed formulation overcomes the above described disadvantages of the current configuration-based model and makes the configuration-based modeling approach more accurate and effective. In general, our model inherits the advantage of day-ahead offer submission convenience for the current configuration-based modeling approach, and at the same time captures the physical constraints for each individual CT and ST in a combined-cycle unit to ensure power system operation feasibility. The detailed contributions of this paper are described as follows:

1) First, our edge-based formulation improves the accuracy of the current configuration-based combined-cycle model by exactly describing the physical constraints of each turbine (in particular, min-up/-down restrictions of each turbine). Due to the accurate modeling, such as tracking the status of each turbine instead of following each configuration as the current configuration-based model does, our edge-based model makes it more flexible to commit units.
2) Second, in terms of computational time, our edge-based formulation performs better than the current configuration-based combined-cycle model, because our model explores the structure of the state transition graph for combined-cycle units (such as the network flow structure) that commercial optimization solvers, e.g., CPLEX, can recognize. Thus, corresponding embedded efficient algorithms developed in these solvers for these types of structures help solve the problem faster.

The remaining part of this paper is organized as follows. Section II explains the basic principle of our edge-based formulation and describes the state transition graphs. Section III provides the details of our mathematical formulation. Section IV incorporates the combined-cycle formulations into the unit commitment problem. Section V reports a case study by comparing our edge-based model with the current configuration-based model. Finally, we summarize our research in Section VI.

II. Edge-Based Modeling Approach

In this section, we review the current configuration-based modeling approach and introduce the basic idea of our edge-based approach.

One important feature for a combined-cycle unit is that the whole unit can work in different configurations because of the STs' dependence on the CTs. This feature makes combined-cycle unit modeling complicated. For example, combined-cycle units with $2\mathrm{CTs} + 1\mathrm{ST}$ have five typical configurations which are $0\mathrm{CT} + 0\mathrm{ST}$, $1\mathrm{CT} + 0\mathrm{ST}$, $2\mathrm{CTs} + 0\mathrm{ST}$, $1\mathrm{CT} + 1\mathrm{ST}$, and

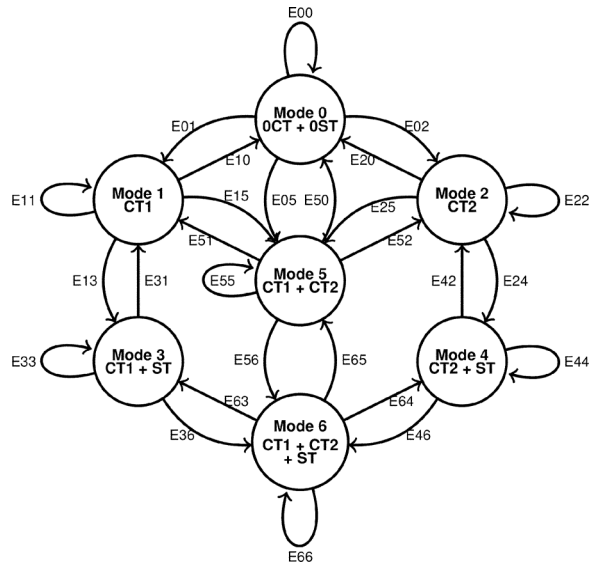

Fig. 1. State transition graph for $2\mathrm{CTs} + 1\mathrm{ST}$.

$2\mathrm{CTs} + 1\mathrm{ST}$. For the current configuration-based modeling approach, each configuration is treated as a pseudo unit with its own physical parameters such as generation limits and ramping rates. Meanwhile, at each operation time period, the combined-cycle unit can only work at one of the configurations. According to the configuration-based modeling approach, the optimization engine for unit commitment in the day-ahead market decides which configuration should be called on at each time period. As the CTs and STs start up or shut down, the combined-cycle unit moves towards different configurations. Based on this, an MILP model, based on configurations, has been introduced to describe the operations of combined-cycle units in [15] and [14]. In this MILP model, each configuration is associated with three binary variables in each time period to indicate its online status, start-up status, and shut-down status in this time period.

Although the current configuration-based modeling approach fits well with the offer/bid submission process, lack of important physical constraints makes operations scheduling difficult due to feasibility issues. In this research, we describe an edge-based modeling approach to keep track of the operating status of each unit such that important physical constraints are captured and the process is operationally convenient. In our model, we distinguish two CTs by numbering them as CT_1 and CT_2 (similarly, $\mathrm{CT}_1, \mathrm{CT}_2, \ldots, \mathrm{CT}_\mathrm{M}$ for the general M CT case), for the convenience of tracking the operating status of each CT. For example, as shown in Fig. 1, combined-cycle units with $2\mathrm{CTs} + 1\mathrm{ST}$ have seven configurations and twenty-seven transition edges. Each edge in the graph represents the transition among configurations. We define binary variables corresponding to the edges in the state transition graph. The values of these binary variables decide the operating status of these configurations. Each node in the graph represents a configuration mode. In total, there are three types of edges: incoming, outgoing, and self-loop edges. For example, in Fig. 2, the edges connected to mode i are divided into three sets. The dashed edges are the incoming edges of mode i, the solid edge is the self-loop edge, and the dotted edges are the outgoing edges of mode i. If any dashed edge or

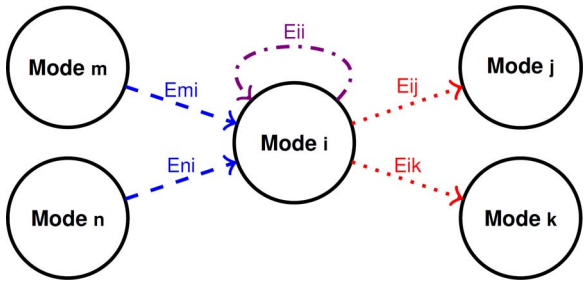

Fig. 2. Edges of one node.

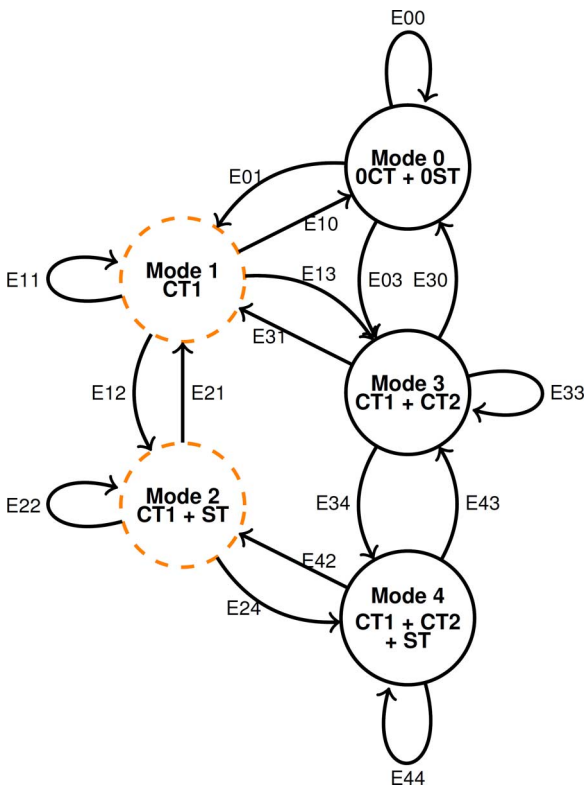

Fig. 3. Reduced state transition graph for 2CTs + 1ST.

dash dotted edge is active, mode i is online. In addition, we define continuous variables to represent the generation amounts for each configuration. The detailed mathematical formulation is described in the next section.

Our state transition graph can be simplified when all CTs in a combined-cycle unit have the same parameters [5]. Because these CTs are identical and symmetric, we can obtain a reduced transition graph by arbitrarily assigning CTs with different priorities. For instance, we let CT_1 have a higher priority than CT_2. That is, we always let CT_1 work rather than CT_2, when only one CT is needed in the combined-cycle unit. In this way, Modes 2 and 4 in Fig. 1 are not needed anymore. Accordingly, the reduced state transition graph of a combined-cycle unit with 2CTs + 1ST can be shown in Fig. 3 with only five modes, for which the number is less than that of the complete state transition graph as shown in Fig. 1. In addition, the number of edges in the reduced state transition graph is reduced to fifteen, which is ten edges less, as compared to the complete state transition

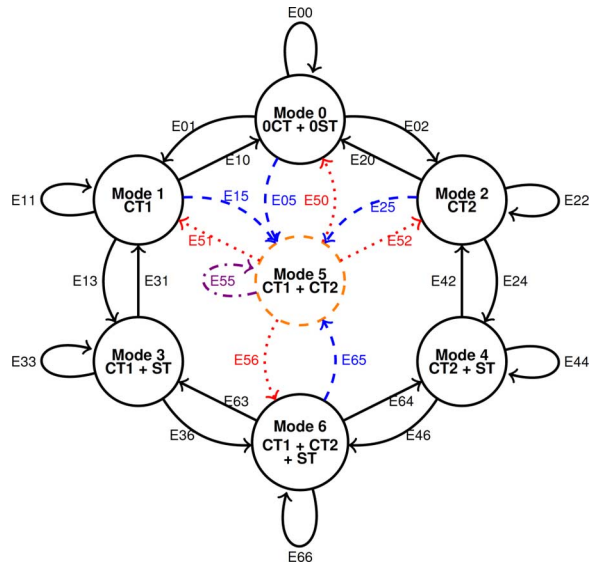

Fig. 4. Logical constraints.

graph. In this way, we can reduce the number of binary variables in the MILP model and speed up the solution process.

III. Math Formulation of a Combined-Cycle Unit

In this section, we focus on analyzing the constraints on combined-cycle unit k and omit the subscript k for notation brevity.

A. Logical Constraints

Accordingly to our state transition analysis in the previous section, the combined-cycle unit moves along one edge during each time period. This means that only one of the edges can be active during each time period, which can be expressed in the following constraints:

$$\sum_{e\in\mathcal{E}} w_e^t = 1, \forall t. \tag{1}$$

In addition, if a mode is online at the current period, in the next time period it can stay in the current mode or move to other modes. For example, as shown in Fig. 4, in order to make Mode 5 online at time period t, one of the incoming dashed or self-loop dash dotted edges should be active at time period t. In the next time period $t+1$, the combined-cycle unit can move along the self-loop dash dotted or outgoing dotted edges. Accordingly, we have the following physical constraints for the combined-cycle unit:

$$\sum_{e\in(\mathcal{E}_m^{\mathrm{in}}\bigcup\mathcal{E}_m^{\mathrm{sl}})} w_e^t = \sum_{e\in(\mathcal{E}_m^{\mathrm{out}}\bigcup\mathcal{E}_m^{\mathrm{sl}})} w_e^{t+1}, \forall m\in\mathcal{M}, \forall t. \tag{2}$$

Note here that if the initial status of the combined-cycle unit is given, which happens in most practices, (2) ensure that only one of the edges can be active at any time period, and accordingly constraints (1) are not needed in our model.

B. Production Costs of a Combined-Cycle Unit

For a given combined-cycle unit, the production cost at each time period is equal to the total production costs of all

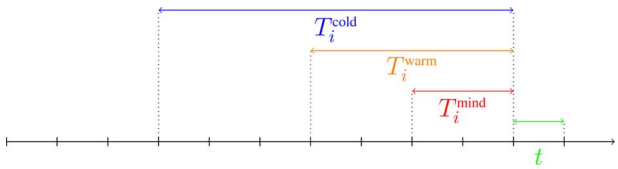

Fig. 5. Offline time.

configurations at each time period as shown in (3):

$$fc^t = \sum_{m \in \mathcal{M}} fc_m^t, \forall t. \tag{3}$$

We treat each mode as a pseudo thermal unit with a quadratic production curve [16]. The quadratic curve can be approximated by a piecewise linear function with N pieces as follows:

$$fc_m^t \geq \alpha_m^n \Big(\sum_{e \in (\mathcal{E}_m^{\text{in}} \bigcup \mathcal{E}_m^{\text{sl}})} w_e^t \Big) + \beta_m^n p_m^t,$$
$$m \in \mathcal{M}, \forall t, n = 1, \ldots, N \tag{4}$$

where α, β are parameters defined in the piecewise linear approximation. In (4), the state of mode m at time period t is represented by the term $\left(\sum_{e \in (\mathcal{E}_m^{\text{in}} \bigcup \mathcal{E}_m^{\text{sl}})} w_e^t \right)$, corresponding to the binary variables of incoming/self-loop edges (i.e., E_{mi}, E_{ni}, and E_{ii} in Fig. 2).

C. Transition Costs of a Combined-Cycle Unit

There are transition costs of a combined-cycle unit at each time period when the transition happens among different modes. That is, there is a transition cost for each incoming/outgoing edge in the graph, which usually denotes the sum of start-up and shut-down costs of the CTs involved in this transition. This cost can be represented as follows:

$$tc^t = \sum_{i \in \mathcal{G}^{\text{CT}}} (suc_i^t + sdc_i^t), \forall t. \tag{5}$$

Note here that there is no transition cost for each self-loop edge. Also, considering the fact that ST is driven by the steam generated by CT(s), the start-up/shut-down costs for STs are not considered in the current setting. However, this framework can be generalized to accommodate these costs easily when needed.

In the following part, we discuss how to calculate start-up and shut-down costs. The start-up cost of a thermal unit is typically a nonlinear nondecreasing function of the "down" time since the last shut-down. This function can be approximated by a stair-wise function [17]. In our formulation, we consider three types of start-up costs (i.e., cold start-up cost, warm start-up cost, and hot start-up cost as shown in Fig. 5) for each CT as follows:

$$suc_i^t \geq \text{SU}_i^{\text{hot}} \sum_{e \in \mathcal{E}_i^{\text{su}}} w_e^t, \forall i \in \mathcal{G}^{\text{CT}}, \forall t, \tag{6}$$

$$suc_i^t \geq \text{SU}_i^{\text{warm}} \Big(\sum_{e \in \mathcal{E}_i^{\text{su}}} w_e^t - \sum_{\tau = T_i^{\text{C,mind}} + 1}^{T_i^{\text{warm}}} \sum_{e \in \mathcal{E}_i^{\text{sd}}} w_e^{t-\tau} \Big),$$
$$\forall i \in \mathcal{G}^{\text{CT}}, \forall t, \tag{7}$$

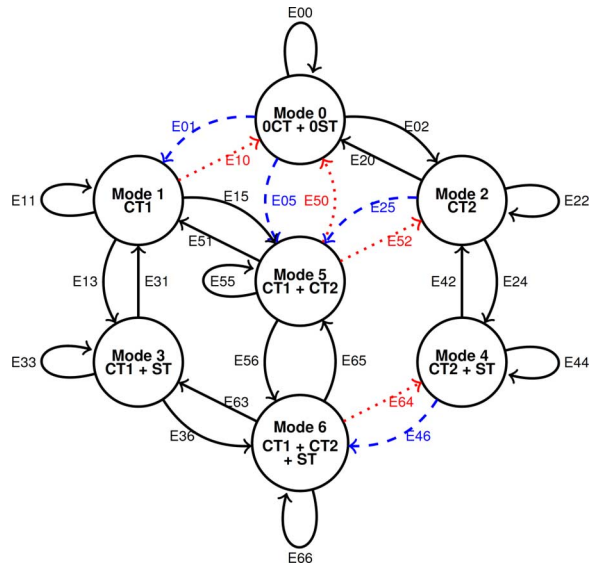

Fig. 6. Start-up costs for CT_1.

$$suc_i^t \geq \text{SU}_i^{\text{cold}} \Big(\sum_{e \in \mathcal{E}_i^{\text{su}}} w_e^t - \sum_{\tau = T_i^{\text{C,mind}} + 1}^{T_i^{\text{cold}}} \sum_{e \in \mathcal{E}_i^{\text{sd}}} w_e^{t-\tau} \Big),$$
$$\forall i \in \mathcal{G}^{\text{CT}}, \forall t \tag{8}$$

where $\text{SU}_i^{\text{hot}}, \text{SU}_i^{\text{warm}}$, and $\text{SU}_i^{\text{cold}}$ represent the hot start-up, warm start-up, and cold start-up costs and $\text{SU}_i^{\text{hot}} < \text{SU}_i^{\text{warm}} < \text{SU}_i^{\text{cold}}$. In formulation (6)–(8), the term $\sum_{e \in \mathcal{E}_i^{\text{su}}} w_e^t$ indicates whether CT_i starts up at time period t. For instance, this term for CT_1, as shown in Fig. 6, is the sum of the binary variables for the dashed edges (i.e., E01, E05, E25, and E46). Once any of these dashed edges becomes active, CT_1 starts up. Similarly, the term $\sum_{e \in \mathcal{E}_i^{\text{sd}}} w_e^{t-\tau}$ indicates if CT_i previously shuts down in time period $t-\tau$. Again, for instance, this term for CT_1 is the sum of the binary variables for the dotted edges (i.e., E10, E50, E52, and E64) in Fig. 6. Now we discuss three cases in terms of when the last shut-down happens, so as to determine the start-up cost for CT_i when it starts up at time period t. First of all, we have $\sum_{e \in \mathcal{E}_i^{\text{su}}} w_e^t = 1$ when CT_i starts up at time period t.

Case 1: if the last shut-down time for CT_i is in a time period between $t - T_i^{\text{warm}}$ and $t - T_i^{\text{C,mind}} - 1$, then the right sides of constraints (7) and (8) are zeros because $\sum_{e \in \mathcal{E}_i^{\text{su}}} w_e^t$, $\sum_{\tau = T_i^{\text{C,mind}} + 1}^{T_i^{\text{warm}}} \sum_{e \in \mathcal{E}_i^{\text{sd}}} w_e^{t-\tau}$, and $\sum_{\tau = T_i^{\text{C,mind}} + 1}^{T_i^{\text{cold}}} \sum_{e \in \mathcal{E}_i^{\text{sd}}} w_e^{t-\tau}$ are all ones. In this case, only constraint (6) is tight and CT_i starts up with a hot start-up cost.

Case 2: if the last shut-down time for CT_i is in a time period between $t - T_i^{\text{cold}}$ and $t - T_i^{\text{warm}} - 1$, then the right sides of constraints (7) and (8) become $\text{SU}_i^{\text{warm}}$ and zero, respectively. In this case, constraint (7) is dominating, because $\text{SU}_i^{\text{hot}} < \text{SU}_i^{\text{warm}}$ and accordingly CT_i starts up with a warm start-up cost.

Case 3: if the last shut-down time for CT_i is beyond the time period $t - T_i^{\text{cold}}$, then the right sides of constraints (7) and (8) become $\text{SU}_i^{\text{warm}}$ and $\text{SU}_i^{\text{cold}}$, respectively. In this case, the constraint (8) is dominating because $\text{SU}_i^{\text{hot}} <$

$\mathrm{SU}_i^{\mathrm{warm}} < \mathrm{SU}_i^{\mathrm{cold}}$, and accordingly CT_i starts up with a cold start-up cost.

The shut-down cost of a CT at each time period can be represented as follows:

$$sdc_i^t = \mathrm{SD}_i \sum_{e \in \mathcal{E}_i^{\mathrm{sd}}} w_e^t, \forall i \in \mathcal{G}^{\mathrm{CT}}, \forall t \tag{9}$$

where term $\sum_{e \in \mathcal{E}_i^{\mathrm{sd}}} w_e^t$ indicates the shut-down action of CT_i.

D. Min-Up Time Constraints

In this section, we formulate the min-up time constraints for each turbine exactly instead of an approximation for each mode in a combined-cycle unit. The constraints can be described as follows:

$$\sum_{e \in \bigcup_{m \in \mathcal{M}_i^{\mathrm{off}}} \mathcal{E}_m^{\mathrm{all}}} w_e^\tau \le 1 - \sum_{e \in \mathcal{E}_i^{\mathrm{su}}} w_e^t, \forall i \in \mathcal{G}^{\mathrm{CT}} \cup \mathcal{G}^{\mathrm{ST}},$$
$$\forall \tau \in \{t+1, \ldots, \min\{\mathcal{T}_{\mathrm{end}}, T_i^{\mathrm{C,minu}} + t - 1\}\}, \forall t. \tag{10}$$

The intuition of these min-up constraints for combined-cycle units is similar to that of the min-up/down constraints for traditional thermal units in [18]. The logic for constraints (10) is that once a turbine starts up, the modes that do not contain this turbine cannot be online for the following consecutive $T_i^{\mathrm{C,minu}}$ time periods or $\mathcal{T}_{\mathrm{end}} - t + 1$ time periods if $\mathcal{T}_{\mathrm{end}} < T_i^{\mathrm{C,minu}} + t - 1$. Note here that this guarantees that turbine i either keeps on for min-up time or hits the end of the operational time horizon because only one of the edges can be active at each time period. For example, as shown in Fig. 7, if any dashed edge (i.e., E01, E05, E25, and E46) is active, which means turbine CT_1 starts up, then the modes where CT_1 is off (solid nodes, i.e., nodes described using solid line cycles, which are Modes 0, 2, and 4) cannot be online at the following min-up time periods. That is, all the edges in Fig. 7 connected to the solid nodes should be inactive in these time periods. Note here that $\bigcup_{m \in \mathcal{M}_i^{\mathrm{off}}} \mathcal{E}_m^{\mathrm{all}}$ represents the set of edges connected to the modes where turbine i is off.

E. Min-Down Time Constraints

Following the same logic, we can formulate the min-down time constraints as follows:

$$\sum_{e \in \bigcup_{m \in \mathcal{M}_i^{\mathrm{on}}} \mathcal{E}_m^{\mathrm{all}}} w_e^\tau \le 1 - \sum_{e \in \mathcal{E}_i^{\mathrm{sd}}} w_e^t, \forall i \in \mathcal{G}^{\mathrm{CT}} \cup \mathcal{G}^{\mathrm{ST}},$$
$$\tau \in \{t+1, \ldots, \min\{\mathcal{T}_{\mathrm{end}}, T_i^{\mathrm{C,mind}} + t - 1\}\}, \forall t. \tag{11}$$

These constraints indicate that if turbine i shuts down in time period t, then the modes that contain this turbine should be offline for consecutive Min-down time periods. The term $\bigcup_{m \in \mathcal{M}_i^{\mathrm{on}}} \mathcal{E}_m^{\mathrm{all}}$ represents the set of the edges connected to modes with turbine i online.

F. Generation Amount Limits

The generation amount of a combined-cycle unit is the sum of all the generation amounts of its modes as shown in (12):

$$p^t = \sum_{m \in \mathcal{M}} p_m^t, \forall t. \tag{12}$$

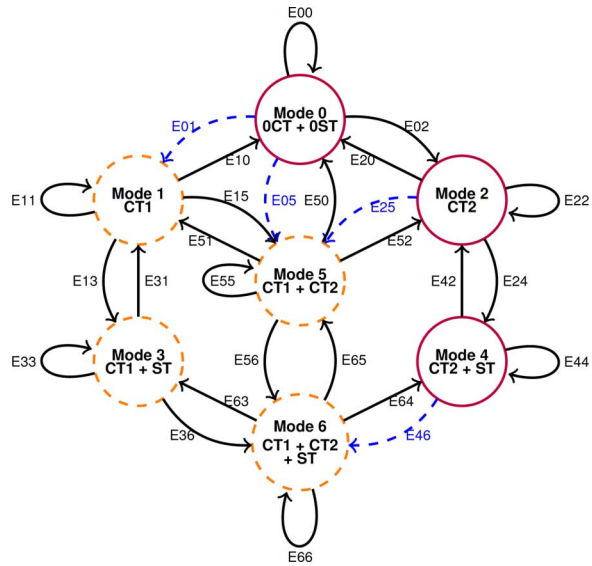

Fig. 7. Min-up time for CT_1.

Each mode as a pseudo-unit has its own generation limits as shown in (13) and (14):

$$P_m^{\min}\Big(\sum_{e \in (\mathcal{E}_m^{\mathrm{in}} \bigcup \mathcal{E}_m^{\mathrm{sl}})} w_e^t\Big) \le p_m^t, \forall m \in \mathcal{M}, \forall t, \tag{13}$$

$$p_m^t \le P_m^{\max}\Big(\sum_{e \in (\mathcal{E}_m^{\mathrm{in}} \bigcup \mathcal{E}_m^{\mathrm{sl}})} w_e^t\Big), \forall m \in \mathcal{M}, \forall t. \tag{14}$$

G. Reserve Constraints

The spinning reserve and operating reserve constraints for a combined-cycle unit are described as follows:

$$p^t + src^t \le \sum_{m \in \mathcal{M}} P_m^{\max}\Big(\sum_{e \in (\mathcal{E}_m^{\mathrm{in}} \bigcup \mathcal{E}_m^{\mathrm{sl}})} w_e^t\Big), \forall t, \tag{15}$$

$$src^t \le \sum_{m \in \mathcal{M}} 10 R_m^{\mathrm{MC}}\Big(\sum_{e \in (\mathcal{E}_m^{\mathrm{in}} \bigcup \mathcal{E}_m^{\mathrm{sl}})} w_e^t\Big), \forall t, \tag{16}$$

$$orc^t - src^t \le C^{\mathrm{QSC}}\Big(\sum_{e \in (\mathcal{E}_m^{\mathrm{in}} \bigcup \mathcal{E}_m^{\mathrm{sl}})} w_e^t\Big), m = 0, \forall t \tag{17}$$

where constraints (15) indicate that the spinning reserve occupies certain capacity for a combined-cycle unit, constraints (16) describe the 10-min spinning reserve capacity, and constraints (17) show the relationship between operating reserve and spinning reserve, following the definitions described in [14], where $m = 0$ represents that all turbines in the combined-cycle unit are offline. The operating reserve is composed of the spinning reserve and the quick start capacity. The quick start capacity is the reserve capacity provided by offline quick-start units. Note here that we can formulate other reserve settings used by different ISOs.

H. Ramping Constraints

Ramping rates of combined-cycle units depend on the system operating status. There are two types of ramping rates. The first refers to the ramping rates within a mode, when a

self-loop edge is active. The second refers to the ramping rates corresponding to the transition between two modes, when an outgoing/incoming edge is active. Accordingly, these ramping rates can be illustrated corresponding to each edge in the graph. Each ramping rate can be 1) the ramping rate for a mode corresponding to each self-loop edge (e.g., edge E55 for Mode 5 in Fig. 8) or 2) the ramping rate for the transition between modes corresponding to outgoing/incoming edges (e.g., edges E05, E50, E15, E51, E25, E52, E56, and E65 for Mode 5 in Fig. 8). The mathematical expression of ramping constraints can be described as follows:

$$p^{t+1} - p^t \le R_e^{\mathrm{U}} w_e^{t+1} + P^{\mathrm{cap}}(1 - w_e^{t+1}), \forall e \in \mathcal{E}, \quad (18)$$

$$p^t - p^{t+1} \le R_e^{\mathrm{D}} w_e^{t+1} + P^{\mathrm{cap}}(1 - w_e^{t+1}), \forall e \in \mathcal{E} \quad (19)$$

where the second term on the right side indicates that if this particular edge is not active (i.e., $w_e^{t+1} = 0$), this ramping constraint is relaxed, following the definition of P^{cap}. Otherwise, if this edge is active (i.e., $w_e^{t+1} = 1$), this edge provides the ramping limit for the whole combined-cycle unit, because only one of the edges can be active at each time period. The intuition to formulate the ramping rate constraints for combined-cycle units is similar to that of the stronger ramping rate constraints developed in [19] for traditional thermal units.

IV. Mathematical Formulation of the Unit Commitment Problem

In this section, we describe the overall formulation for the general network constrained unit commitment problem including both traditional thermal and combined-cycle units.

A. Objective Function

The objective includes the operational costs of traditional thermal units and combined-cycle units, which can be described as follows:

$$\min \sum_{t\in\mathcal{T}} \sum_{n\in\mathcal{G}^{\mathrm{T}}} \left(\mathrm{SU}_n u_n^t + \mathrm{SD}_n v_n^t + ft_n^t\right) + \sum_{t\in\mathcal{T}} \sum_{k\in\mathcal{G}^{\mathrm{C}}} (fc_k^t + tc_k^t). \quad (20)$$

Note here that similar as fc_k^t, the quadratic production cost for each traditional thermal unit, ft_n^t can be approximated by a piece-wise linear function with additional constraints.

Besides constraints (2)–(19) presented in Section III for each combined-cycle unit, we have the following constraints for the whole system.

B. Constraints for a Traditional Thermal Unit

Constraints for traditional thermal units can be described as follows:

$$u_n^t + v_n^t \le 1, \forall n \in \mathcal{G}^{\mathrm{T}}, \forall t, \quad (21)$$

$$y_n^t - y_n^{t-1} = u_n^t - v_n^t, \forall n \in \mathcal{G}^{\mathrm{T}}, \forall t, \quad (22)$$

$$\sum_{\tau=t-T_n^{\mathrm{T,minu}}+1}^{t} u_n^\tau \le y_n^t, \quad \forall n \in \mathcal{G}^{\mathrm{T}}, \forall t \in \{T_n^{\mathrm{T,minu}}, \ldots, \mathcal{T}_{\mathrm{end}}\}, \quad (23)$$

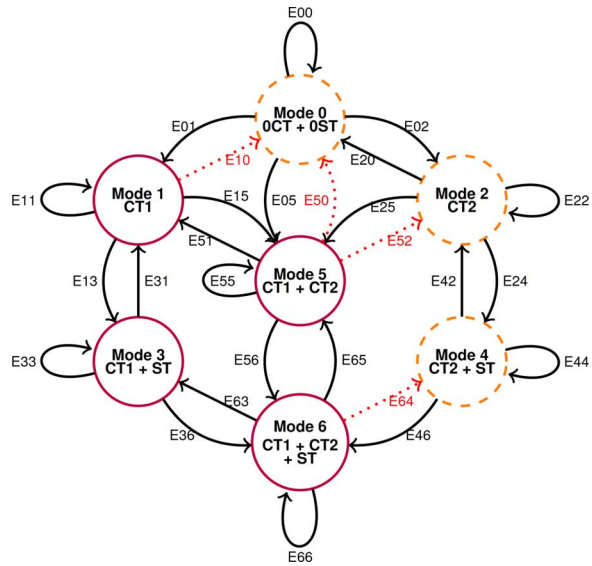

Fig. 8. Min-down time for CT_1.

$$\sum_{\tau=t-T_n^{\mathrm{T,mind}}+1}^{t} v_n^\tau \le 1 - y_n^t, \quad \forall n \in \mathcal{G}^{\mathrm{T}}, \forall t \in \{T_n^{\mathrm{T,mind}}, \ldots, \mathcal{T}_{\mathrm{end}}\}, \quad (24)$$

$$P_n^{\min} y_n^t \le p_n^t \le P_n^{\max} y_n^t, \forall n \in \mathcal{G}^{\mathrm{T}}, \forall t, \quad (25)$$

$$p_n^t - p_n^{t-1} \le R_n^{\mathrm{U}} y_n^{t-1} + \overline{R}_n^{\mathrm{U}} u_n^t, \forall n \in \mathcal{G}^{\mathrm{T}}, \forall t, \quad (26)$$

$$p_n^{t-1} - p_n^t \le R_n^{\mathrm{D}} y_n^t + \overline{R}_n^{\mathrm{D}} v_n^t, \forall n \in \mathcal{G}^{\mathrm{T}}, \forall t, \quad (27)$$

$$srt_n^t \le 10 R_n^{\mathrm{MT}} y_n^t, \forall n \in \mathcal{G}^{\mathrm{T}}, \forall t, \quad (28)$$

$$srt_n^t + p_n^t \le P_n^{\max}, \forall n \in \mathcal{G}^{\mathrm{T}}, \forall t, \quad (29)$$

$$ort_n^t - srt_n^t \le (1 - y_n^t) C_n^{\mathrm{QST}}, \forall n \in \mathcal{G}^{\mathrm{T}}, \forall t, \quad (30)$$

$$u_n^t, v_n^t, y_n^t \in \{0, 1\}, \forall n \in \mathcal{G}^{\mathrm{T}}, \forall t$$

where constraints (21) and (22) represent the relationships between the operating statuses and start-up/shut-down operations. Constraints (23) and (24) describe the minimum up/down time restrictions. Constraints (25) represent the generation limits of traditional thermal units. Constraints (26) and (27) express the ramping rate limits. Constraints (28) and (29) indicate the spinning reserve limits. Constraints (30) describe the operating reserve of a traditional thermal unit, which is restricted by its quick start capacity and spinning reserve amount.

C. System Energy Balance and Reserve Constraints

$$\sum_{n\in\mathcal{G}^{\mathrm{T}}} p_n^t + \sum_{k\in\mathcal{G}^{\mathrm{C}}} p_k^t - \sum_{b\in\mathcal{B}} \mathrm{D}_b^t = 0, \forall t, \quad (31)$$

$$\sum_{n\in\mathcal{G}^{\mathrm{T}}} srt_n^t + \sum_{k\in\mathcal{G}^{\mathrm{C}}} src_k^t \ge \mathrm{RS}^t, \forall t, \quad (32)$$

$$\sum_{n\in\mathcal{G}^{\mathrm{T}}} ort_n^t + \sum_{k\in\mathcal{G}^{\mathrm{C}}} orc_k^t \ge \mathrm{RO}^t, \forall t. \quad (33)$$

In the above constraints, besides the power balance constraints described in (31), constraints (32) and (33) describe the overall spinning and operating reserve requirements.

TABLE I
COMPUTATIONAL RESULTS FOR COMBINED-CYCLE UNITS WITH TRANSMISSION CONSTRAINTS

Inst	MIPObj ($)				IGap (%)				Time(s)				TGap(10^{-2})		Nnodes				Niterations			
	REBM	CEBM	CCBM	CBM	REBM	CEBM	CCBM	CBM	REBM	CEBM	CCBM	CBM	CCBM	CBM	REBM	CEBM	CCBM	CBM	REBM	CEBM	CCBM	CBM
FL	1890961	1890958	1897559	1905418	0.09	0.09	0.92	0.58	826.22	1404.15	***	***	0.21	0.03	4322	3712	6258	22333	441803	375723	2332668	3588068
1	1891207	1891199	1897423	1905634	0.09	0.09	0.90	0.58	1331.52	2078.50	***	***	0.20	0.03	6443	5051	8907	28460	778141	521283	2403488	4147401
2	1895120	1895113	1900834	1909580	0.09	0.09	0.87	0.58	1025.23	2041.36	***	***	0.16	0.04	5091	4648	7569	27111	637139	565508	2308836	4448649
3	1893582	1893528	1899374	1908078	0.09	0.09	0.87	0.58	667.57	1429.95	***	***	0.14	0.03	4213	3829	7241	26053	369909	444657	2026841	3718824
4	1894464	1894457	1900471	1908931	0.09	0.09	0.89	0.59	671.21	1991.50	***	***	0.16	0.04	4173	4293	8412	33749	401861	423199	2281645	4304629
5	1893758	1893747	1899424	1908154	0.09	0.09	0.87	0.57	722.27	1406.53	***	***	0.14	0.03	3710	3546	8157	35659	395214	551171	2337376	4049542
6	1896392	1896388	1902415	1910833	0.09	0.09	0.89	0.58	641.79	1701.63	***	***	0.17	0.03	4049	3680	8036	36129	328758	536488	2398858	4230499
7	1895057	1895055	1901002	1909643	0.09	0.10	0.89	0.59	1236.84	2044.27	***	***	0.18	0.04	4870	4944	9362	18622	636946	557657	2408343	3372375
8	1885881	1885881	1891808	1900277	0.08	0.09	0.88	0.58	609.92	1557.85	***	***	0.17	0.03	3641	4601	6852	22587	343994	560078	2379102	2589879
9	1888290	1888260	1894009	1902627	0.09	0.09	0.88	0.58	1158.91	2493.35	***	***	0.18	0.04	5084	4118	7188	27085	684522	619940	2802640	3719726
10	1895621	1895617	1902574	1910061	0.09	0.10	0.94	0.58	1391.27	1830.58	***	***	0.25	0.04	4537	3952	6843	25510	534596	490667	2786803	4322060

TABLE II
COMPUTATIONAL RESULTS FOR COMBINED-CYCLE UNITS WITHOUT TRANSMISSION CONSTRAINTS

Inst	MIPObj ($)				IGap (%)				Time(s)				TGap(10^{-2})		Nnodes				Niterations			
	REBM	CEBM	CCBM	CBM	REBM	CEBM	CCBM	CBM	REBM	CEBM	CCBM	CBM	CCBM	CBM	REBM	CEBM	CCBM	CBM	REBM	CEBM	CCBM	CBM
FL	1876273	1876268	1882078	1891750	0.07	0.07	0.86	0.57	132.06	924.64	***	***	0.17	0.03	610	17754	23755	36069	100735	742009	7621614	1998651
1	1875769	1875769	1881543	1891286	0.07	0.07	0.86	0.56	98.14	425.25	***	***	0.17	0.03	50	3815	27131	35573	1669	600727	4887711	2335787
2	1879861	1879856	1885691	1895387	0.07	0.07	0.86	0.56	124.11	397.62	***	***	0.17	0.03	281	3453	20848	35439	7207	251458	5803832	2317992
3	1878829	1878819	1884607	1894306	0.07	0.07	0.86	0.56	66.96	652.96	***	***	0.15	0.03	453	6901	26163	35622	11367	463577	5051979	2398824
4	1879265	1879238	1885000	1894623	0.07	0.07	0.86	0.57	80.4	463.4	***	***	0.18	0.03	153	3641	26786	35274	4059	359806	5915907	2377133
5	1878916	1878847	1884758	1894391	0.07	0.07	0.87	0.57	114.05	258.64	***	***	0.16	0.02	110	3413	25822	35632	2732	247952	4815514	2130666
6	1881532	1881513	1887268	1897059	0.07	0.07	0.86	0.56	127.28	497.66	***	***	0.16	0.03	545	3699	28140	36136	17796	399642	5008776	2598757
7	1879637	1879637	1885453	1895182	0.07	0.07	0.86	0.56	130.86	458.07	***	***	0.16	0.03	384	4341	19424	35476	9758	294628	7507280	2146055
8	1871193	1871192	1876921	1886560	0.07	0.07	0.86	0.56	213.33	783.13	***	***	0.17	0.03	3326	13210	23340	36043	181317	637106	5373936	2484997
9	1873008	1872999	1878762	1888443	0.07	0.07	0.86	0.56	138.9	438.58	***	***	0.18	0.03	2388	3635	27575	35583	52268	288597	4699745	2306739
10	1880030	1879987	1885707	1895532	0.07	0.07	0.85	0.56	94.57	314.66	***	***	0.16	0.03	342	3261	20080	35569	10564	411595	6857421	2435495

D. Transmission Constraints

$$\sum_{n\in\mathcal{G}_b^{\mathrm{T}}} p_n^t + \sum_{k\in\mathcal{G}_b^{\mathrm{C}}} p_k^t - \mathrm{D}_b^t - \sum_{(b,l)\in\mathcal{L}} \frac{\theta_b^t - \theta_l^t}{X_{b,l}} = 0, \forall b \in \mathcal{B}, \forall t, \tag{34}$$

$$-C_{b,l} \le \frac{\theta_b^t - \theta_l^t}{X_{b,l}} \le C_{b,l}, \forall (b,l) \in \mathcal{L}, \forall t. \tag{35}$$

Constraints (34) indicate the power balance at each bus. Constraints (35) describe transmission line limits.

V. CASE STUDIES

In this section, we implement the computational experiments to compare our edge-based model with the configuration-based model and component-based model (CBM) proposed in [14] and [15] through testing the modified IEEE 118-bus system (online at [20]). The system contains 54 traditional thermal units and 12 combined-cycle units. We use commercial optimization solver CPLEX 12.5 to solve the unit commitment (UC) problem at an Intel(R) Core(TM) i7–4500U 1.8 GHz with 8G memory.

In our experiment, we let the operational horizon be 24 h and each time unit be 30 min. We compare four approaches: the current configuration-based model (CCBM), the component-based model (CBM), the complete edge-based model (CEBM), and the reduced edge-based model (REBM). We report the computational performance (including computational time) of each approach in the following Section V-A. In Section V-B, we analyze the actual combinations of CTs and the ST obtained in these four approaches to show the flexibility of our approach, and perform the Monte Carlo simulation to evaluate the cost savings of our approach.

A. Computational Performance

In this subsection, we report the computational performance of each approach with and without considering transmission constraints in Tables I and II. Given the load forecasts $\bar{D}^t$, we generate 10 different load profiles of $D^t(i), i = 1, \ldots, 10$ by following the method described in [21] and [22], in which the error ϵ^t between random variable D^t and $\bar{D}^t$ follows a Gaussian distribution with mean zero and standard deviation $\bar{D}^t/100$. In the third row of each table, we report the computational performance for $\bar{D}^t$ (denoted as "FL"). Then, in the next ten rows, we report the computational performance for the ten instances of $D^t(i), i = 1, \ldots, 10$.

For each modeling approach, we report the optimal objective value of the mixed-integer-linear program (denoted as "MIPObj"). Furthermore, we calculate the integrality gap (denoted as "IGap") between MIPObj and LPObj (the optimal objective value of the linear programming relaxation) to show the tightness of each formulation. More specifically, the integrality gap can be calculated as follows:

$$\mathrm{IGap} = \frac{\mathrm{MIPObj} - \mathrm{LPObj}}{\mathrm{MIPObj}} \times 100\%. \tag{36}$$

We also report the computational time for each approach to solve the problem into optimality (denoted as "Time (s)"). In our case study, the default CPLEX optimality gap (0.01%) is utilized and the time limit is 5400 s. In Tables I and II, we use "***" to indicate if CPLEX cannot solve the instance within the time limit (e.g., see the column labelled "CBM" in the "Time (s)" category). Accordingly, for this case, we report the terminating gap (e.g., see the column labelled "TGap (10^{-4})"). We also report the number of branching nodes in the branch-and-bound tree (denoted as "Nnodes") and the number of simplex iterations (denoted as "Niterations"). From these tables, we can observe

TABLE III
SCHEDULES OF COMBINED-CYCLE UNITS WITH TRANSMISSION CONSTRAINTS

CCI		Time Periods (1-13)													Time Periods (14-48)
4001/4002 4007/4009	EBM	1	3	6	6	6	6	6	6	6	6	6	6	6	6
	CBM	1	1	3	6	6	6	6	6	6	6	6	6	6	6
	CCBM	1	1	1	1	3	3	3	3	6	6	6	6	6	6
4003	EBM	1	3	6	6	6	6	6	6	6	6	6	6	6	6
	CBM	2	2	4	4	4	4	4	6	6	6	6	6	6	6
	CCBM	1	1	1	1	3	3	3	3	6	6	6	6	6	6
4004	EBM	0	0	0	0	0	0	1	3	6	6	6	6	6	6
	CBM	0	0	0	2	2	4	4	6	6	6	6	6	6	6
	CCBM	5	5	5	5	6	6	6	6	6	6	6	6	6	6
4005	EBM	1	3	6	6	6	6	6	6	6	6	6	6	6	6
	CBM	1	1	3	6	6	6	6	6	6	6	6	6	6	6
	CCBM	5	5	5	5	6	6	6	6	6	6	6	6	6	6
4006	EBM	1	3	6	6	6	6	6	6	6	6	6	6	6	6
	CBM	2	2	4	4	4	6	6	6	6	6	6	6	6	6
	CCBM	1	1	1	1	3	3	3	3	6	6	6	6	6	6
4008	EBM	1	3	6	6	6	6	6	6	6	6	6	6	6	6
	CBM	2	2	4	6	6	6	6	6	6	6	6	6	6	6
	CCBM	1	1	1	1	3	3	3	3	3	3	3	3	6	6
4010	EBM	0	0	0	0	0	1	3	3	6	6	6	6	6	6
	CBM	0	0	0	0	2	2	4	6	6	6	6	6	6	6
	CCBM	1	1	1	1	3	3	3	3	3	3	3	3	3	6
4011	EBM	0	0	0	0	1	3	6	6	6	6	6	6	6	6
	CBM	0	0	2	2	4	6	6	6	6	6	6	6	6	6
	CCBM	1	1	1	1	3	3	3	3	6	6	6	6	6	6
4012	EBM	1	3	6	6	6	6	6	6	6	6	6	6	6	6
	CBM	2	2	4	4	6	6	6	6	6	6	6	6	6	6
	CCBM	1	1	1	1	3	3	3	3	3	6	6	6	6	6

TABLE IV
SCHEDULES OF COMBINED-CYCLE UNITS WITHOUT TRANSMISSION CONSTRAINTS

CCI		Time Periods (1-9)									Time Periods (10 - 48)
4001	EBM	0	0	0	0	1	3	6	6	6	6
	CBM	0	0	0	2	2	4	6	6	6	6
	CCBM	0	1	1	1	1	3	3	3	3	6
4002 4005 4009	EBM	1	3	6	6	6	6	6	6	6	6
	CBM	1	1	3	6	6	6	6	6	6	6
	CCBM	1	1	1	1	3	3	3	3	6	6
4003 4006	EBM	1	3	6	6	6	6	6	6	6	6
	CBM	1	1	3	3	6	6	6	6	6	6
	CCBM	1	1	1	1	3	3	3	3	6	6
4004	EBM	0	0	0	0	0	1	3	6	6	6
	CBM	0	0	1	1	3	6	6	6	6	6
	CCBM	1	1	1	1	3	3	3	3	6	6
4007 4008 4012	EBM	1	3	6	6	6	6	6	6	6	6
	CBM	2	2	4	6	6	6	6	6	6	6
	CCBM	5	5	5	5	6	6	6	6	6	6
4010	EBM	0	0	0	0	0	1	3	6	6	6
	CBM	0	0	0	1	1	3	6	6	6	6
	CCBM	1	1	1	1	3	3	3	3	6	6
4011	EBM	0	0	0	0	0	1	3	6	6	6
	CBM	0	0	0	1	1	3	6	6	6	6
	CCBM	1	1	1	1	3	3	3	3	3	6

TABLE V
OPERATING COSTS OF DAY-AHEAD SCHEDULES

Inst	Models	WTC				WOTC	
		Mean ($)		STD ($)		Mean ($)	STD ($)
1	CEBM	1891398		3551		1876228	3354
	REBM	1891370		3551		1876231	3356
	CCBM	1897900		3544		1882038	3365
	CBM	1905833		3587		1891748	3404
		Mean ($)		STD ($)		Mean ($)	STD ($)
		$5k/MWh	$10k/MWh	$5k/MWh	$10k/MWh		
2	CEBM	2310962	2353726	39557	77080	2226418	3997
	REBM	2310974	2353735	39557	77081	2226405	3998
	CCBM	2341086	2401947	45424	88895	2236823	4003
	CBM	2332378	2375647	39675	77257	2246475	4031

that the running times of REBM and CEBM are shorter in each instance because of their smaller IGaps.

B. Schedule Results Analysis

In Tables III and IV, we report the schedules of combined-cycle units obtained by four modeling approaches for $\bar{D}^t$ to show the flexibility of our approach. Column 1, labelled "CCI", displays the indices of combined-cycle units (i.e., from 4001 to 4012). The next column shows the names of four modeling approaches. Because the schedules of combined-cycle units produced by CEBM and REBM are the same, we use EBM to represent CEBM and REBM. The remaining columns report the unit commitment schedules for each combined-cycle unit in terms of modes. Note here that, in our case study, each combined-cycle unit $(2\ \mathrm{CTs} + 1\ \mathrm{ST})$ has seven modes in the CEBM approach as shown in Fig. 1. However, in REBM and CCBM, each combined-cycle unit has five modes as shown in Fig. 3, in which we assume that CT_1 is always picked when only one CT is needed to work. In this way, the set of modes for REBM and CCBM is a subset of those for CEBM. Accordingly, it is sufficient to set the mode indices of the combination results of CTs and ST for these four approaches as follows: Mode $0 \rightarrow 0\ \mathrm{CT} + 0\ \mathrm{ST}$, Mode $1 \rightarrow \mathrm{CT}_1$, Mode $2 \rightarrow \mathrm{CT}_2$, Mode $3 \rightarrow \mathrm{CT}_1 + \mathrm{ST}$, Mode $4 \rightarrow \mathrm{CT}_2 + \mathrm{ST}$, Mode $5 \rightarrow \mathrm{CT}_1 + \mathrm{CT}_2$, and Mode $6 \rightarrow \mathrm{CT}_1 + \mathrm{CT}_2 + \mathrm{ST}$.

From Tables III and IV, we can observe that the combined-cycle units, modeled by EBM (i.e., CEBM or REBM) and CBM, are more flexible because these three approaches provide min-up/down time constraints for each turbine instead of each mode. As an illustration, we analyze the scheduling results of combined-cycle unit 4001 obtained from different approaches in Table III. For CCBM, this unit has to stay in Mode 1 from time period 1 to time period 4, because the min-up time for Mode 1 is assumed to be four time periods in CCBM. Similarly, this unit has to stay at Mode 3 from time period 5 to time period 8, because the min-up time for Mode 3 is also 4. Therefore, in order to reach the most economical Mode 6 in the optimal solution for CCBM, combined-cycle unit 4001 has to wait 8 time periods. On the other hand, due to flexibility, EBM (i.e., CEBM or REBM) can make combined-cycle unit 4001 reach Mode 6 in time period 3 in the optimal solution for these two approaches. After CT_1 is started up, this unit can start ST at time period 2, as long as the min-down time of ST is satisfied and finally, this unit can reach Mode 6 at time period 3. The start-up process of combined-cycle unit 4001 in CBM is similar to those of EBM.

From Tables I and II, we can observe that the costs of CEBM and REBM are lower than that of CCBM for each instance. These case study results verify that our CEBM and REBM approaches allow more flexibility in combined-cycle unit commitment. This flexibility finally leads to lower costs if the load is deterministic, as compared to CCBM.

We further perform Monte Carlo simulations to test the performances of four different modeling approaches (i.e., CEBM, REBM, CCBM, and CBM) in terms of total operating costs when the load is uncertain. The total operating costs include the load curtailment costs. We utilize the Monte Carlo simulation framework described in [22] to generate the samples, and the number of required samples is calculated by following

TABLE VI
LOAD CURTAILMENT COSTS OF DAY-AHEAD SCHEDULES

Inst	Models	WTC			
		$5k/MWh		$10k/MWh	
		Mean ($)	STD ($)	Mean ($)	STD ($)
2	CEBM	42777	37653	85500	75285
	REBM	42777	37654	85508	75284
	CCBM	60824	43607	121530	87174
	CBM	43290	37722	86511	75419

TABLE VII
EMPIRICAL PROBABILITY DISTRIBUTIONS OF OPERATING COSTS

Inst			Intervals	CEBM	REBM	CBM	CCBM
1	WOTC		[$1882940, +∞)	0.02	0.02	0.995	0.398
			[$1879584, $1882940)	0.149	0.149	0.004	0.362
			[$1876228, $1879584)	0.335	0.335	0.001	0.204
			[$1869517, $1872873)	0.129	0.129	0	0.004
			[$1872873, $18762228)	0.344	0.344	0	0.032
			[$0, $1869517)	0.023	0.023	0	0
	WTC		[$1898499, +∞)	0.02	0.02	0.979	0.434
			[$1894949, $1898499)	0.143	0.144	0.02	0.358
			[$1891398, $1894949)	0.333	0.33	0.001	0.179
			[$1887847, $1891398)	0.342	0.34	0	0.028
			[$1884296, $1887847)	0.141	0.145	0	0.001
			[$0, $1884296)	0.021	0.021	0	0
2	WOTC		[$2234413, +∞)	0.018	0.018	0.999	0.714
			[$2230416, $2234413)	0.152	0.152	0.001	0.231
			[$2226418, $2230416)	0.336	0.336	0	0.048
			[$2222421, $2226418)	0.337	0.337	0	0.007
			[$2218423, $2222421)	0.134	0.134	0	0
			[$0, $2218423)	0.023	0.023	0	0
	WTC	VoLL $5k/MWh	[$2390076, +∞)	0.037	0.037	0.083	0.134
			[$2350519, $2390076)	0.11	0.11	0.202	0.243
			[$2310962, $2350519)	0.288	0.288	0.352	0.335
			[$2271405, $2310962)	0.405	0.405	0.363	0.281
			[$0, $2271405)	0.16	0.16	0	0.007
	WTC	VoLL $10k/MWh	[$2507886, +∞)	0.037	0.037	0.055	0.106
			[$2430806, $2507886)	0.115	0.115	0.161	0.231
			[$2353726, $2430806)	0.281	0.281	0.326	0.321
			[$2276645, $2353726)	0.394	0.394	0.457	0.315
			[$0, $2276645)	0.173	0.173	0.001	0.027

the method described in [23]. In our approach, the real-time unit commitment decisions are allowed in these Monte Carlo simulations and the optimization software CPLEX is set at its default setting. We test two different load forecast instances as shown in Table V. The first instance is the same as instance "FL" as described in Tables I and II in Section VI-A. In this instance, there is no load curtailment for both cases with and without transmission constraints (WTC and WOTC), because every scenario in the simulation is feasible when the real-time unit commitment decisions are considered. The second instance triggers load curtailments when transmission constraints are incorporated into the unit commitment model (i.e., WTC). In this case, we run the simulations under two different values of lost load ($5000/MWh [24] and $10 000/MWh). The data for both instances can be found in [20]. The computational results, including the mean value and standard deviation (STD) of operating costs and load curtailment costs, are reported in Tables V and VI. From Table V, we can observe the cost savings of our approach in terms of the total operating costs as compared to CCBM. The similar results in terms of the load curtailment costs can be observed in Table VI. In addition, REBM has almost the same costs as CEBM does. This indicates that REBM is a better model for most practices because

TABLE VIII
EMPIRICAL PROBABILITY DISTRIBUTIONS OF LOAD CURTAILMENT COSTS

Inst			Intervals	CEBM	REBM	CBM	CCBM
2	WTC	VoLL $5k/MWh	[$155735, +∞)	0.01	0.01	0.01	0.029
			[$118082, $155735)	0.027	0.027	0.028	0.064
			[$80430, $118082)	0.114	0.114	0.117	0.211
			[$42777, $80430)	0.282	0.282	0.283	0.303
			[$5124, $42777)	0.386	0.386	0.39	0.319
			[$0, $5124)	0.181	0.181	0.172	0.074
		VoLL $10k/MWh	[$311354,+∞)	0.01	0.01	0.01	0.029
			[$236069, $311354)	0.027	0.027	0.028	0.064
			[$160785, $236069)	0.116	0.116	0.118	0.21
			[$85500, $160785)	0.28	0.28	0.281	0.304
			[$10216, $85500)	0.386	0.386	0.391	0.319
			[$0, $10216)	0.181	0.181	0.172	0.074

it takes less time to solve the problem. Finally, we report the empirical probability distributions of the operating costs and load curtailment costs in Tables VIII and VIII in Appendix A.

VI. CONCLUSIONS

In this paper, we improved the current configuration-based model of the combined-cycle units by proposing the edge-based model. Our proposed model can accommodate the day-ahead offer submission process and meanwhile ensure the power system operation feasibility by capturing the detailed physical constraints for each CT and ST in the combined-cycle unit.

We first described the transition process of the combined-cycle units as a graph and introduced binary variables for each edge. With the help of these edge-based binary variables, we formulated the detailed physical constraints including min-up/down time, ramping, and start-up/shut-down operational constraints, and the time dependent start-up costs for each turbine in the combined-cycle units. Furthermore, we reduced the complete edge-based model into a more efficient one with fewer decision variables when the characteristics of CTs are similar in the combined-cycle units. Finally case studies verified that our edge-based model had a better computational performance than the current configuration-based model.

APPENDIX
EMPIRICAL PROBABILITY DISTRIBUTIONS OF COSTS

Table VII lists the empirical probability distributions of operating costs, and Table VIII lists the empirical probability distributions of load curtailment costs.

ACKNOWLEDGMENT

The authors would like to thank the editor and referees for their sincere suggestions and L. Wei for his insightful discussions on the mathematical formulation of combined-cycle units. The authors would also like to thank X. Wang from Alstom and Y. Chen from MISO for their constructive comments and suggestions.

REFERENCES

[1] Energy Perspectives 1949–2011 [Online]. Available: http://www.eia.gov/totalenergy/data/annual/perspectives.cfm
[2] B. Lu and M. Shahidehpour, "Short-term scheduling of combined cycle units," *IEEE Trans. Power Syst.*, vol. 19, no. 3, pp. 1616–1625, Aug. 2004.

[3] R. Kehlhofer, B. Rukes, F. Hannemann, and F. Stirnimann, *Combined-Cycle Gas & Steam Turbine Power Plants*. Tulsa, OK, USA: Pennwell, 2009.
[4] N. Troy, D. Flynn, and M. O'Malley, "Multi-mode operation of combined-cycle gas turbines with increasing wind penetration," *IEEE Trans. Power Syst.*, vol. 27, no. 1, pp. 484–492, Feb. 2012.
[5] M. Tamayo, X. Yu, X. Wang, and J. Zhang, "Configuration based combined cycle model in market resource commitment," in *Proc. 2013 IEEE Power and Energy Soc. General Meeting*, pp. 1–5.
[6] G. Anders, P. Eng, I. N. England, and A. Morched, *Commitment Techniques for Combined-Cycle Generating Units*. Toronto, ON, Canada: Kinectrics , 2005.
[7] H. Hui, C.-N. Yu, F. Gao, and R. Surendran, "Combined cycle resource scheduling in ERCOT nodal market," in *Proc. 2011 IEEE Power and Energy Soc. General Meeting*, pp. 1–8.
[8] J. Alvarez Lopez, R. N. Gómez, and I. G. Moya, "Commitment of combined cycle plants using a dual optimization-dynamic programming approach," *IEEE Trans. Power Syst.*, vol. 26, no. 2, pp. 728–737, May 2011.
[9] M-35 Definitions and Abbreviations [Online]. Available: http://www.iso-ne.com/participate/rules-procedures/manuals
[10] B. Blevins, "Combined-cycle unit modeling in the nodal design," ERCOT. Taylor, TX, USA, 2007 [Online]. Available: http://www.ercot.com/content/meetings/tptf/keydocs/2007/0611/18a1_IDA00Combined_Cycle_Whitepaper_v.91.doc
[11] M. Smith, "Combined cycle modeling in MRTU—the challenges," *Calpine* Nov. 2008 [Online]. Available: http://www.caiso.com
[12] A. Papavasiliou, Y. He, and A. Svoboda, "Self-commitment of combined cycle units under electricity price uncertainty," *IEEE Trans. Power Syst.*, to be published.
[13] H. Hui, "Reliability unit commitment in ERCOT nodal market," Ph.D. dissertation, Univ. Texas at Arlington, Arlington, TX, USA, 2013.
[14] C. Liu, M. Shahidehpour, Z. Li, and M. Fotuhi-Firuzabad, "Component and mode models for the short-term scheduling of combined-cycle units," *IEEE Trans. Power Syst.*, vol. 24, no. 2, pp. 976–990, May 2009.
[15] T. Li and M. Shahidehpour, "Price-based unit commitment: a case of Lagrangian relaxation versus mixed integer programming," *IEEE Trans. Power Syst.*, vol. 20, no. 4, pp. 2015–2025, Nov. 2005.
[16] A. J. Wood and B. F. Wollenberg, *Power Generation, Operation, and Control*. New York, NY, USA: Wiley, 2012.
[17] M. Carrión and J. M. Arroyo, "A computationally efficient mixed-integer linear formulation for the thermal unit commitment problem," *IEEE Trans. Power Syst.*, vol. 21, no. 3, pp. 1371–1378, Aug. 2006.
[18] D. Rajan and S. Takriti, "Minimum up/down polytopes of the unit commitment problem with start-up costs," *IBM Res. Rep.*, 2005.
[19] J. Ostrowski, M. F. Anjos, and A. Vannelli, "Tight mixed integer linear programming formulations for the unit commitment problem," *IEEE Trans. Power Syst.*, vol. 27, no. 1, pp. 39–46, Feb. 2012.
[20] IEEE 118-bus System [Online]. Available: https://sites.google.com/site/leifanee/dataset/
[21] M. A. Ortega-Vazquez and D. S. Kirschen, "Estimating the spinning reserve requirements in systems with significant wind power generation penetration," *IEEE Trans. Power Syst.*, vol. 24, no. 1, pp. 114–124, Feb. 2009.
[22] M. A. Ortega-Vazquez and D. S. Kirschen, "Assessing the impact of wind power generation on operating costs," *IEEE Trans. Smart Grid*, vol. 1, no. 3, pp. 295–301, 2010.
[23] G. Hahn and S. Shapiro, *Statistical Models in Engineering*, ser. Wiley Series on Systems Engineering and Analysis Series. New York, NY, USA: Wiley, 1967.
[24] A. Papavasiliou, S. Oren, and R. O'Neill, "Reserve requirements for wind power integration: A scenario-based stochastic programming framework," *IEEE Trans. Power Syst.*, vol. 26, no. 4, pp. 2197–2206, Nov. 2011.

Lei Fan (S'13) received the B.S. degree in electrical engineering from the Hefei University of Technology, Hefei, China, in 2009. He is currently pursuing the Ph.D. degree in the Department of Industrial and Systems Engineering at the University of Florida, Gainesville, FL, USA.

His research interests include optimization of power system operations and energy market analysis.

Yongpei Guan (M'10–SM'13) received the B.S. degree in mechanical engineering and economic decision science from the Shanghai Jiao Tong University, Shanghai, China, in 1998, the M.S. degree in industrial engineering and engineering management from the Hong Kong University of Science and Technology, Hong Kong, China, in 2001, and the Ph.D. degree in industrial and systems engineering from the Georgia Institute of Technology, Atlanta, GA, USA, in 2005.

He is currently the Director of the Computational and Stochastic Optimization Lab at the University of Florida, Gainesville, FL, USA. His research interests include power system operations and energy policy analysis.